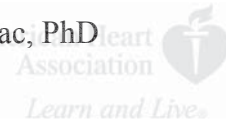# Spatial Profiles of Electrical Mismatch Determine Vulnerability to Conduction Failure across a Host-Donor Cell Interface

Running title: *Kirkton et al.; Conduction Failure across Host-Donor Interface*

Robert D. Kirkton, PhD; Nima Badie, PhD; Nenad Bursac, PhD

Department of Biomedical Engineering, Duke University, Durham, NC

Correspondence:

Nenad Bursac, PhD

Associate Professor

Department of Biomedical Engineering

Duke University

Room 136 Hudson Hall

Durham, NC 27708

Tel: 919-660-5510

Fax: 919-684-4488

E-mail: nbursac@duke.edu

Abstract:

Background - Electrophysiological mismatch between host cardiomyocytes and donor cells can directly affect the electrical safety of cardiac cell therapies; however, the ability to study host-donor interactions at the microscopic scale *in situ* is severely limited. We systematically explored how action potential (AP) differences between cardiomyocytes and other excitable cells modulate vulnerability to conduction failure *in vitro*.

Methods and Results - AP propagation was optically mapped at 75 μm resolution in micropatterned strands (n=152) in which host neonatal rat ventricular myocytes (NRVMs; AP duration (APD)=153.2±2.3 ms, conduction velocity (CV)=22.3±0.3 cm/s) seamlessly interfaced with genetically engineered excitable donor cells expressing inward rectifier potassium (Kir2.1) and cardiac sodium ($Na_v1.5$) channels with either weak (CV=3.1±0.1 cm/s) or strong (CV=22.1±0.4 cm/s) electrical coupling. Selective prolongation of engineered donor cell APD (from 31.9-139.1 ms) by low dose $BaCl_2$ generated a wide range of host-donor repolarization time (RT) profiles with maximum gradients (∇RT_{max}) of 5.5-257 ms/mm. During programmed stimulation of donor cells, the vulnerable time window (VW) for conduction block across the host-donor interface most strongly correlated with ∇RT_{max}. Compared to well-coupled donor cells, the interface composed of poorly-coupled cells significantly shortened the RT profile width by 19.7% and increased ∇RT_{max} and VW by 22.2% and 19%, respectively. Flattening the RT profile by perfusion of 50 μmol/L $BaCl_2$ eliminated coupling-induced differences in vulnerability to block.

Conclusions - Our results quantify how the degree of electrical mismatch across a cardiomyocyte-donor cell interface affects vulnerability to conduction block with important implications for the design of safe cardiac cell and gene therapies.

Introduction

Clinical trials of stem cell therapy for myocardial infarction and heart failure have demonstrated encouraging but mixed results.[1, 2] While the field is rapidly advancing, our abilities to understand therapeutic mechanisms and predict potential adverse outcomes (eg, cardiac arrhythmias) remain inadequate.[3, 4] Specifically, understanding how a mismatch in the electrical properties of donor cells and host cardiomyocytes affects cardiac function is becoming critically important with the advent of pluripotent stem cell-[5-7] or direct reprogramming-[8-10] derived cardiomyocytes as these cells are both electrically excitable and able to couple to host heart tissue. While understanding the arrhythmogenic consequences of host-donor electrical mismatch is essential to the rational design of safe and efficient cell therapies, our ability to systematically study these conditions *in situ* is limited by low reproducibility of cardiac tissue microstructure and function among different hearts and the inability to access, identify, and directly study heterocellular interactions within the complex setting of the heart.

Previously, we utilized micropatterned cocultures of neonatal rat ventricular myocytes (NRVMs) and passive unexcitable cells (eg, mesenchymal stem cells, skeletal myoblasts, cardiac fibroblasts, wild-type human embryonic kidney 293 (HEK293) cells) to study the roles of heterocellular gap junctional coupling[11] in cardiac action potential (AP) shape[12] and conduction.[13] Similarly, micropatterned NRVM strands were used by others to examine the influence of passive cells (cultured on top of[14] or inserted within[15] the strand) on cardiomyocyte spontaneous activity and AP propagation. While these studies have improved our understanding of the effects that endogenous or implanted unexcitable cells may have on cardiac electrical activity, the potential deleterious effects of *in situ* reprogrammed or exogenously implanted excitable cells (eg, cardiomyocytes) have not been systematically explored. Specifically,

quantifying how host-donor mismatch in basic electrophysiological properties (ie, conduction velocity, AP duration) can cause or alleviate electrical disturbance in the heart would provide a rationale for tailoring (eg, by genetic[16] or biochemical[17] means) the electrical properties of newly emerging excitable cells[5-10] towards safer and more effective cardiac cell therapies.

In this study, we generated micropatterned heterocellular strands in which host neonatal rat cardiomyocytes on one half of the strand formed a seamless and easily identifiable interface with genetically engineered excitable donor cells that occupied the other half of the strand. While not suitable for clinical applications, monoclonally-derived engineered cell lines with reproducible and well-defined electrical properties allowed us to create a wide range of host-donor mismatch conditions *in vitro* to systematically investigate their roles in safety of AP conduction. In particular, we set to test the hypothesis that vulnerability to conduction failure across a cardiomyocyte-donor cell interface is governed by an interplay of AP duration and strength of electrical coupling in donor cells.

Methods

Micropatterned fibronectin lines[13] (Figure I in the online-only Data Supplement) and a polydimethylsiloxane (PDMS) frame were used to create 150 μm-wide homocellular ("host" or "donor") or heterocellular ("host-donor") strands (Figure 1). Host cells in the strands were represented by NRVMs while donor cells were represented by one of two genetically engineered excitable HEK293 monoclonal cell lines: 1) the poorly-coupled "Excitable Slow" or "ExS" engineered HEK293 cell line stably expressing human voltage-gated cardiac sodium (Na$_v$1.5) and inward rectifier potassium (Kir2.1) channels and 2) the well-coupled "Excitable Fast" or "ExF" engineered HEK293 cell line derived by the additional stable expression of rat connexin-43 (Cx43) gap junctions.[18] Action potential propagation along the strands was optically mapped

at 10x magnification using a voltage-sensitive dye (ANNINE-6plus).[19] An S1-S2 pacing protocol

was applied to the donor cells to study vulnerability to conduction block across the interface

between host NRVMs and donor excitable HEK293 cells. An expanded Methods section is

provided in the online-only Data Supplement.

Results

Optical mapping in Heterocellular Host-Donor Strands

The stable expression of fluorescent reporters in ExS (GFP, mCherry) and ExF (GFP, mCherry,

mOrange) donor cells (Figure III in the online-only Data Supplement) allowed us to exactly

localize the host-donor interface in co-cultured strands (Figure 2A) and, under 10x

magnification, align and spatially register strands with recording sites from an optical fiber array

(Figure 2B). Intense membrane staining of the cells with the voltage sensitive dye, ANNINE-

6plus,[19] further revealed the differences in size (smaller vs. larger) and geometry (round vs.

elongated) in donor cells vs. host NRVMs. (Figure 2B). Immunostaining showed the existence of

a seamless interface between the two cell types with Cx43 gap junctions found between NRVMs

and ExF (but not ExS) cells (Figure IIID in the online-only Data Supplement). The difference

("mismatch") between the APD of the ExF or ExS donor cells (31.9±0.7 or 34.6±1.1 ms,

respectively) and that of the host NRVMs (153.2±2.3 ms) yielded the formation of a monotonic

APD profile (APD change along the strand) that extended over a length of ~1.2 mm across the

host-donor interface (Figure 2B, and Figure IVA and IVB, Movie I in the online-only Data

Supplement).

Pacing from the donor end of ExF-NRVM strands resulted in unhindered conduction

across the heterocellular interface (Figure 2C) as evidenced by equally spaced activation

isochrones and linear increase in activation time (AT) indicative of the robust intercellular

coupling and similar CVs between the host NRVM and donor ExF cells (22.3±0.3 and 22.1±0.4

cm/s, respectively). In contrast, the poorly-coupled ExS cells (ie, electrically connected by weak

endogenous HEK293 gap junctions other than Cx43)[18] displayed significantly slower CV

(3.1±0.1 cm/s) as evidenced by dense activation isochrones and a steep AT slope compared to

NRVMs, thereby creating a sharp change in the activation gradient at the ExS-NRVM interface

(Figure 2D). The spatial profiles of APD and repolarization time (RT, obtained by

superimposing AT and APD profiles, Figure 2C and 2D, bottom) across the host-donor interface

were quantified by measuring the width (Δx APD and Δx RT), height (Δy APD and Δy RT), and

maximum slope (gradient, ∇APD_{max} and ∇RT_{max}) during 2 Hz stimulation (Figure IVC in the

online-only Data Supplement). As expected, the significant APD difference (Δy APD=~100-105

ms) between the donor cells and host NRVMs generated sharp repolarization profiles (with

∇RT_{max}=~150-200 ms/mm) that extended over a relatively short distance (Δx RT=~0.5-0.6 mm).

Furthermore, pacing of the same strands from the host NRVM end resulted in specific changes in

the shape of AT and RT profiles (Figure V in the online-only Data Supplement).

Effect of BaCl$_2$ on Electrical Mismatch at the Host-Donor Interface

We have previously shown that inhibition of inward rectifier K$^+$ current (I_{K1}) by BaCl$_2$ can

significantly prolong the APD of excitable HEK293 cells.[18] In this study, we utilized low doses

of BaCl$_2$ as a method to selectively and reproducibly prolong the APD of donor cells without

affecting the electrical properties of host NRVMs (Figure II and Table I in the online-only Data

Supplement). In particular, the addition of 25 or 50 µmol/L BaCl$_2$ during 2 Hz stimulation from

the donor cell end of heterocellular strands (see Movie III in the online-only Data Supplement)

resulted in the flattening of the APD profile (ie, reduction of APD mismatch) at the host-donor

interface (Figure 3A-C). When quantified (Figure 3D-I), the application of 25 and 50 µmol/L

$BaCl_2$ significantly and progressively decreased the height and maximum slope and increased the width of both APD and RT profiles in host-donor strands. For example, adding 50 µmol/L $BaCl_2$ to ExS-NRVM strands, decreased ∇RT_{max} and Δy RT by an average of 83.4% and 67.2%, respectively, while Δx RT increased by an average of 98.1%.

Compared to ExF-NRVM strands, ExS-NRVM strands in 0 µmol/L $BaCl_2$ had significantly smaller Δx APD (0.52 vs. 0.64 mm) and Δx RT (0.53 vs. 0.66 mm) and significantly larger ∇APD_{max} (186 vs. 164 ms/mm) and ∇RT_{max} (201 vs. 165 ms/mm). Therefore, due to reduced coupling in ExS vs. ExF cells, the spatial profiles of APD and RT mismatch were significantly steeper and narrower at the ExS-NRVM interface than at the ExF-NRVM interface. Interestingly, upon application of either concentration of $BaCl_2$, the significant differences between the APD and RT profile parameters of ExF-NRVM and ExS-NRVM strands were annulled. Thus, the application of low doses of $BaCl_2$ enabled us to selectively vary the shape parameters of APD and RT profiles over a wide range of values (eg, ∇RT_{max} between 5.5-256.9 ms/mm) without altering activation time profiles in any of the strands. Higher doses of $BaCl_2$ caused APD prolongation in NRVMs and CV reduction in all cells, likely by depolarizing membrane potential and reducing Na^+ current availability, as previously shown by others[20] and us.[18]

Occurrence of Conduction Block at the Host-Donor Interface

Application of a progressively more premature S2 stimulus from the donor end of the heterocellular strands eventually resulted in S2 conduction block at the host-donor interface. In ExF-NRVM strands, block occurred significantly after (0.29±0.06 mm) the host-donor interface as compared to ExS-NRVM strands where the block occurred before (0.07±0.03 mm) the interface (Figure 4A-C). While the site of block in the ExF-NRVM strands also occurred

significantly past ∇RT_{max} (by 0.37 ± 0.06 mm), in ExS-NRVM strands, block co-localized with

the site of ∇RT_{max} (Figure 4D). With reduction of the S1-S2 interval below the maximum S1-S2

interval at which block occurred (S1-S2$_{max}$), the position of S2 conduction block progressively

shifted towards the donor cell end of the strand (Figure 4E and 4F). Below a certain S1-S2 value,

these conduction blocks across the host-donor interface converted into a local 2:1 block at the

pacing site. The time difference between S1-S2$_{max}$ that yielded conduction block across the host-

donor interface and S1-S2$_{max}$ that resulted in 2:1 block at the pacing site was measured as the

vulnerable time window (VW) for conduction block (Figure VI in the online-only Data

Supplement).

Shape of Host-Donor Mismatch Profile Determines Vulnerability to Conduction Block

The use of two different donor cell lines (ExS and ExF) and BaCl$_2$ doses with selective action on

donor cells allowed us to vary and systematically study how the shape of the spatial profile of

electrical host-donor mismatch affects the vulnerability to conduction block during premature

excitation (Figure 5). Overall, the vulnerable time window for conduction block (VW) increased

with an increase in Δy RT or ∇RT_{max} and decreased with an increase in Δx RT (Figure 5A-C).

∇RT_{max} was the only parameter that significantly (and with the highest r^2) correlated with VW

across all BaCl$_2$ doses (Figure 5C), while Δy RT and Δx RT showed significant correlation with

VW for either lower ∇RT_{max} (50 µmol/L BaCl$_2$, Figure 5A) or higher ∇RT_{max} (0 and 25 µmol/L

BaCl$_2$, Figure 5B) values, respectively (see Table II in the online-only Data Supplement). At 50

µmol/L BaCl$_2$, the critical (smallest) ∇RT_{max} that still precipitated block across the host-donor

interface was 5.5-7.9 ms/mm. Moreover, the poorly-coupled ExS-NRVM strands had a

significantly longer VW compared to the well-coupled ExF-NRVM strands in both 0 µmol/L

BaCl$_2$ (153.9 ± 1.4 ms vs. 129.3 ± 2.5 ms, respectively) and 25 µmol/L BaCl$_2$ (113.7 ± 3.3 ms vs.

93.4±2.3 ms, respectively) but not when the ∇RT_{max} was largely reduced with 50 µmol/L BaCl$_2$

(42.2±3.4 ms vs. 30.4±4.8 ms, P=0.06, Figure 5D). Interestingly, at 25 µmol/L BaCl$_2$, VW was

found to be significantly higher in ExS-NRVM than ExF-NRVM strands despite no difference in

their APD and RT mismatch profiles (Figure 3D-I).

Effect of Intercellular Coupling on Conduction Block at the Host-Donor Interface

An unexpected finding of this study was that propagation from the ExS end of ExS-NRVM

strands was blocked across the host-donor interface at higher S1-S2$_{max}$ intervals than when the

same strand was paced from the NRVM end (Figure 6A). This increased vulnerability to

conduction block across the host-donor interface, as compared to pacing site blocks at the host or

donor ends of the strand, was characteristic for ExS-NRVM but not ExF-NRVM strands (data

not shown). With addition of BaCl$_2$, this increased vulnerability to block was diminished and the

BaCl$_2$ treated cells were now able to sustain propagation at a lower S1-S2$_{max}$ (Figure 6B and see

Movie IV in the online-only Data Supplement). Comparing the S1-S2$_{max}$ over multiple strands

(Figure 6C) showed that the increased vulnerability to block across the interface in ExS-NRVM

strands was reduced to the levels measured in ExF-NRVM strands by selectively increasing the

APD in donor cells by addition of 50 µmol/L BaCl$_2$.

Discussion

Previous experimental studies in healthy canine hearts have reported maximum APD gradients

from ~5-8 ms/mm across the ventricular wall[21, 22] to ~25 ms/mm in the crista terminalis.[23] In

diseased hearts, these gradients can increase dramatically to ~120 ms/mm[22, 24, 25] and enhance the

vulnerability to conduction block and arrhythmias. Similarly, in excitable cell-based cardiac

therapies, differences in APD and CV between implanted donor cells (eg, human skeletal

myotubes[26] with APD of ~8 ms, human pluripotent stem cell-derived cardiomyocytes[4, 27-29] with

APD of ~120-510 ms and CV of ~1-25 cm/s, or human fibroblast-reprogrammed cardiomyocytes[10] with APD of ~280-390 ms) and host cardiomyocytes (APD of ~270-440 ms and CV of ~41-50 cm/s)[30-32] can generate a wide range of electrical gradients that may be additionally modulated by host-donor differences in resting membrane potential, cell geometry, and intercellular coupling.[4, 27, 28] Moreover, excitable pluripotent- or reprogramming-derived cardiogenic cell sources are known to have heterogeneous and temporally changing electrical phenotypes[10, 33] (ie, variation in channel expression, AP properties, cell coupling), thus adding to the potential complexity of APD and CV host-donor mismatch *in situ*.

We thus created a novel host-donor strand assay in which a wide range of APD gradients (~6-280 ms/mm) at two distinct levels of cell coupling were reproducibly generated between excitable donor cells (ExF and ExS) and NRVMs. This well-controlled *in vitro* setting, representative of potential electrical heterogeneities found in cell therapy-treated hearts, allowed us to systematically study how electrical mismatch across a cardiomyocyte-donor cell interface influences AP conduction and vulnerability to block. Specifically, by mapping the AP propagation at microscopic scale, we for the first time quantified the precise roles that shape of the spatial profile of repolarization in heterocellular cardiac tissue has upon the vulnerability to conduction block during premature excitation. We also determined how reduced coupling in donor cells affects the shape of activation and repolarization profiles at the host-donor cell interface, as well as the propensity to and exact location of the conduction block. Through these studies, we further uncovered the antagonistic effects of APD prolongation and reduced coupling in donor cells on successful conduction of premature beats.

The sharpest spatial profiles of host-donor electrical mismatch and highest vulnerability to S1-S2 conduction block in our study were observed when using the ExS donor cells with poor

coupling that reduced the width and increased the slope of the RT profile (Figure 3H and 3I). In these ExS-NRVM strands, S2 conduction block occurred near the host-donor interface at the site of ∇RT_{max}, in contrast to well-coupled ExF-NRVM strands where block always occurred at a position past the interface and ∇RT_{max} (Figure 4A-D). These results are in general agreement with *in situ* observations from diseased hearts with reduced coupling[24, 25] and simulated well-coupled cardiac cables with a preset APD profile.[34] Furthermore, with decrease of S1-S2 interval, the position of S2 block in all host-donor strands shifted into the donor cell region towards the stimulus site (Figure 4E-F), as a direct result of the altered amount of source current available for the depolarization of downstream tissue (electrical sink). Specifically, a sharper repolarization gradient or shorter S1-S2 interval reduced the diastolic interval and available source current earlier during propagation thereby dynamically increasing the source-sink mismatch and yielding the observed shift of conduction block towards the pacing site.

An important result of this study was that of all the parameters used to characterize the shape of host-donor mismatch profiles, ∇RT_{max} most strongly correlated with the vulnerable window for conduction block (Figure 5C and Table II in the online-only Data Supplement). Several experimental[24, 25, 35] and theoretical[34, 36] studies have shown that larger ∇RT_{max} resulted in an increased VW, but the exact quantitative relationship between ∇RT_{max} and VW over a wide range of APD profile shapes has not been previously described. Furthermore, previous experiments in intact hearts and cardiac tissue wedge preparations suggested that the lowest ∇RT_{max} yielding unidirectional conduction block and reentry induction is between 3.2-12.5 ms/mm[24, 25, 35], which is consistent with our results in ExF-NRVM strands showing no block for $\nabla RT_{max} < 7.9$ ms/mm (ie, Δy APD < 9.8 ms). This agreement between different *in vivo* and *in vitro* studies suggests that the dimensionality of tissue setting (eg, pseudo-1-D in strands vs. 3-D

in intact tissue) and the underlying cause of the spatial APD profile (eg, host-donor interface vs. ion channel heterogeneity) may be a lesser determinant of the vulnerability to block than the general shape parameters of the mismatch profile (eg, maximum gradient). We also found overall correlation between the magnitude of VW and Δy RT, but within each $BaCl_2$ dose, this correlation was significant only for the smallest APD gradients when Δy APD was reduced below ~55 ms (Figure 5A). In a simulated cable of ventricular myocytes, Qu et al. also observed positive linear correlation between Δy RT and VW[36] for relatively small Δy APD<~50 ms and predicted that VW will continue to linearly increase with increasing Δy APD, consistent with our results.

Interestingly, in 25 µmol/L $BaCl_2$, the shapes of the mismatch profiles between ExS-NRVM and ExF-NRVM strands were comparable (Figure 3D-I), however VW was still significantly larger in ExS-NRVM strands (Figure 5D), suggesting that cell-coupling dependent differences in activation profile and associated source-sink mismatch at the host-donor interface also contributed to the vulnerability to conduction block. This higher vulnerability to block in the poorly coupled ExS-NRVM vs. well-coupled ExF-NRVM strands was fully eliminated by further increasing the donor cell APD by application of 50 µmol/L $BaCl_2$. Similar results were observed when comparing the $S1-S2_{max}$ for conduction block at the host-donor interface vs. pacing site block at the NRVM region (Figure 6C). This result likely reflected the inability of the poorly-coupled donor cells to, during long intercellular delays, transfer a sufficient amount of excitatory current into the larger and well-coupled NRVMs to sustain active propagation. While $BaCl_2$-induced prolongation of APD in the donor cells shortened the diastolic interval during S2 propagation (Figure 6B), it also reduced the source-sink mismatch at the ExS-NRVM interface rendering its $S1-S2_{max}$ similar to that in the NRVM-only region, thereby eliminating the VW

difference between ExS-NRVM and ExF-NRVM strands. Mechanistically, these results are consistent with previous observations that prolonging APD decreased the likelihood of conduction block in poorly coupled cells[37] or abrupt tissue expansions.[38]

Therapeutic Implications

Our study primarily explored how host-donor mismatch in APD and electrical coupling affects vulnerability to conduction block when an AP is propagated from excitable donor cells into host cardiomyocytes. This *in vitro* setting most directly pertains to the potential therapeutic use of electrically active donor cells (eg, those derived from human pluripotent stem cells)[7-9] that typically have an immature cardiomyocyte phenotype with significantly smaller size, reduced APD and CV, and increased propensity to ectopic activity compared to adult ventricular myocytes.[4-6, 27] Moreover, the results of our study would directly relate to potential therapies with primary human somatic cells (eg, dermal or cardiac fibroblasts) engineered to become electrically active.[18, 39] In the above therapeutic scenarios with excitable donor cells, our studies suggest that vulnerability to conduction block during premature excitation would be additively increased by a low APD and CV (due to reduced cell coupling) of donor cells compared to that of the host cardiomyocytes. Selective APD modification in donor cells (eg, by the genetic modification of ion channel expression[16] or specific differentiation protocols[6, 17]) to reduce repolarization mismatch at the host-donor interface appears to be the most effective strategy to reduce vulnerability to conduction failure as well as to offset the detrimental effects of weak donor cell coupling. Furthermore, our studies suggest that under well-coupled (but not poorly-coupled) conditions, perfect matching of donor with host APD is not required to prevent occurrence of block at the host-donor interface during premature excitation. When our results are scaled up by fold-difference in human vs. neonatal rat ventricular APD, the maximum APD

mismatch not leading to block at a human host-donor interface would amount to ~25 ms.

Study Limitations

The most obvious limitation of this study is the currently unavoidable use of neonatal cardiomyocytes and the simplified *in vitro* nature of our experimental preparation. Specifically, compared to our study, the 3-D nature of native tissue along with significantly greater resting input impedance of adult vs. neonatal myocytes (due to larger cell size, K^+ current density, and presence of T-tubules) is expected to augment electrotonic loading and increase vulnerability to conduction block at a host-donor interface in the adult myocardium. Furthermore, while we utilized the pseudo-1-D geometric setting of cell strands to effectively track microscopic conduction across the host-donor cell interface, this setting did not allow for examination of whether the observed conduction block would eventually yield arrhythmia induction. The use of tissue engineering techniques to generate a more realistic 2-D or 3-D host-donor interface[40] is expected to facilitate more accurate studies of AP conduction and arrhythmogenesis as well as guide the future design of safer and more efficient cardiac cell therapies. Finally, while in this report we focused on systematically varying and studying host-donor differences in fundamental electrical properties (ie, APD and CV), further studies are needed to elucidate the specific roles that host-donor mismatch in individual ion currents, calcium handling, and cell size and geometry would play in vulnerability to conduction block and arrhythmias.

Conflict of Interest Disclosures: None.

References:

1. Delewi R, Andriessen A, Tijssen JG, Zijlstra F, Piek JJ, Hirsch A. Impact of intracoronary cell therapy on left ventricular function in the setting of acute myocardial infarction: A meta-analysis of randomised controlled clinical trials. *Heart*. 2013;99:225-232.

2. Jeevanantham V, Butler M, Saad A, Abdel-Latif A, Zuba-Surma EK, Dawn B. Adult bone marrow cell therapy improves survival and induces long-term improvement in cardiac parameters: A systematic review and meta-analysis. *Circulation*. 2012;126:551-568.

3. Tongers J, Losordo DW, Landmesser U. Stem and progenitor cell-based therapy in ischaemic heart disease: Promise, uncertainties, and challenges. *Eur Heart J*. 2011;32:1197-1206.

4. Chen HS, Kim C, Mercola M. Electrophysiological challenges of cell-based myocardial repair. *Circulation*. 2009;120:2496-2508.

5. Mandel Y, Weissman A, Schick R, Barad L, Novak A, Meiry G, Goldberg S, Lorber A, Rosen MR, Itskovitz-Eldor J, Binah O. Human embryonic and induced pluripotent stem cell-derived cardiomyocytes exhibit beat rate variability and power-law behavior. *Circulation*. 2012;125:883-893.

6. Mummery CL, Zhang J, Ng ES, Elliott DA, Elefanty AG, Kamp TJ. Differentiation of human embryonic stem cells and induced pluripotent stem cells to cardiomyocytes: A methods overview. *Circ Res*. 2012;111:344-358.

7. Shiba Y, Fernandes S, Zhu WZ, Filice D, Muskheli V, Kim J, Palpant NJ, Gantz J, Moyes KW, Reinecke H, Van Biber B, Dardas T, Mignone JL, Izawa A, Hanna R, Viswanathan M, Gold JD, Kotlikoff MI, Sarvazyan N, Kay MW, Murry CE, Laflamme MA. Human es-cell-derived cardiomyocytes electrically couple and suppress arrhythmias in injured hearts. *Nature*. 2012;489:322-325.

8. Qian L, Huang Y, Spencer CI, Foley A, Vedantham V, Liu L, Conway SJ, Fu JD, Srivastava D. In vivo reprogramming of murine cardiac fibroblasts into induced cardiomyocytes. *Nature*. 2012;485:593-598.

9. Song K, Nam YJ, Luo X, Qi X, Tan W, Huang GN, Acharya A, Smith CL, Tallquist MD, Neilson EG, Hill JA, Bassel-Duby R, Olson EN. Heart repair by reprogramming non-myocytes with cardiac transcription factors. *Nature*. 2012;485:599-604.

10. Wada R, Muraoka N, Inagawa K, Yamakawa H, Miyamoto K, Sadahiro T, Umei T, Kaneda R, Suzuki T, Kamiya K, Tohyama S, Yuasa S, Kokaji K, Aeba R, Yozu R, Yamagishi H, Kitamura T, Fukuda K, Ieda M. Induction of human cardiomyocyte-like cells from fibroblasts by defined factors. *Proc Natl Acad Sci U S A*. 2013;110:12667-12672.

11. Pedrotty DM, Klinger RY, Badie N, Hinds S, Kardashian A, Bursac N. Structural coupling of cardiomyocytes and noncardiomyocytes: Quantitative comparisons using a novel micropatterned cell pair assay. *Am J Physiol Heart Circ Physiol*. 2008;295:H390-400.

12. McSpadden LC, Nguyen H, Bursac N. Size and ionic currents of unexcitable cells coupled to cardiomyocytes distinctly modulate cardiac action potential shape and pacemaking activity in micropatterned cell pairs. *Circ Arrhythm Electrophysiol*. 2012;5:821-830.

13. Klinger R, Bursac N. Cardiac cell therapy in vitro: Reproducible assays for comparing the efficacy of different donor cells. *IEEE Eng Med Biol Mag*. 2008;27:72-80.

14. Miragoli M, Gaudesius G, Rohr S. Electrotonic modulation of cardiac impulse conduction by myofibroblasts. *Circ Res*. 2006;98:801-810.

15. Gaudesius G, Miragoli M, Thomas SP, Rohr S. Coupling of cardiac electrical activity over extended distances by fibroblasts of cardiac origin. *Circ Res*. 2003;93:421-428.

16. Lieu DK, Fu JD, Chiamvimonvat N, Tung KC, McNerney GP, Huser T, Keller G, Kong CW, Li RA. Mechanism-based facilitated maturation of human pluripotent stem cell-derived cardiomyocytes. *Circ Arrhythm Electrophysiol*. 2013;6:191-201.

17. Zhang Q, Jiang J, Han P, Yuan Q, Zhang J, Zhang X, Xu Y, Cao H, Meng Q, Chen L, Tian T, Wang X, Li P, Hescheler J, Ji G, Ma Y. Direct differentiation of atrial and ventricular myocytes from human embryonic stem cells by alternating retinoid signals. *Cell Res*. 2011;21:579-587.

18. Kirkton RD, Bursac N. Engineering biosynthetic excitable tissues from unexcitable cells for electrophysiological and cell therapy studies. *Nat Commun*. 2011;2:300.

19. Fromherz P, Hubener G, Kuhn B, Hinner MJ. Annine-6plus, a voltage-sensitive dye with good solubility, strong membrane binding and high sensitivity. *Eur Biophys J*. 2008;37:509-514.

20. Chan YC, Tse HF, Siu CW, Wang K, Li RA. Automaticity and conduction properties of bio-artificial pacemakers assessed in an in vitro monolayer model of neonatal rat ventricular myocytes. *Europace*. 2010;12:1178-1187.

21. Yan GX, Shimizu W, Antzelevitch C. Characteristics and distribution of m cells in arterially perfused canine left ventricular wedge preparations. *Circulation*. 1998;98:1921-1927.

22. Poelzing S, Rosenbaum DS. Altered connexin43 expression produces arrhythmia substrate in heart failure. *American journal of physiology. Heart and circulatory physiology*. 2004;287:H1762-1770.

23. Spach MS, Dolber PC, Anderson PA. Multiple regional differences in cellular properties that regulate repolarization and contraction in the right atrium of adult and newborn dogs. *Circ Res*. 1989;65:1594-1611.

24. Restivo M, Gough WB, el-Sherif N. Ventricular arrhythmias in the subacute myocardial infarction period. High-resolution activation and refractory patterns of reentrant rhythms. *Circ Res*. 1990;66:1310-1327.

25. Akar FG, Rosenbaum DS. Transmural electrophysiological heterogeneities underlying arrhythmogenesis in heart failure. *Circ Res*. 2003;93:638-645.

26. Iannaccone ST, Li KX, Sperelakis N. Transmembrane electrical characteristics of cultured human skeletal muscle cells. *J Cell Physiol*. 1987;133:409-413.

27. Blazeski A, Zhu R, Hunter DW, Weinberg SH, Boheler KR, Zambidis ET, Tung L. Electrophysiological and contractile function of cardiomyocytes derived from human embryonic stem cells. *Prog Biophys Mol Biol*. 2012;110:178-195.

28. Hoekstra M, Mummery CL, Wilde AA, Bezzina CR, Verkerk AO. Induced pluripotent stem cell derived cardiomyocytes as models for cardiac arrhythmias. *Frontiers in physiology*. 2012;3:346.

29. Zhang D, Shadrin IY, Lam J, Xian HQ, Snodgrass HR, Bursac N. Tissue-engineered cardiac patch for advanced functional maturation of human esc-derived cardiomyocytes. *Biomaterials*. 2013;34:5813-5820.

30. Glukhov AV, Fedorov VV, Lou Q, Ravikumar VK, Kalish PW, Schuessler RB, Moazami N, Efimov IR. Transmural dispersion of repolarization in failing and nonfailing human ventricle. *Circ Res*. 2010;106:981-991.

31. Koller ML, Maier SK, Gelzer AR, Bauer WR, Meesmann M, Gilmour RF, Jr. Altered dynamics of action potential restitution and alternans in humans with structural heart disease. *Circulation*. 2005;112:1542-1548.

32. Drouin E, Charpentier F, Gauthier C, Laurent K, Le Marec H. Electrophysiologic characteristics of cells spanning the left ventricular wall of human heart: Evidence for presence of m cells. *J Am Coll Cardiol*. 1995;26:185-192.

33. Ivashchenko CY, Pipes GC, Lozinskaya IM, Lin Z, Xu X, Needle S, Grygielko E, Hu E, Toomey J, Lepore J, Willette RN. Human induced pluripotent stem cell derived cardiomyocytes exhibit temporal changes in phenotype. *Am J Physiol Heart Circ Physiol*. 2013

34. Sampson KJ, Henriquez CS. Simulation and prediction of functional block in the presence of structural and ionic heterogeneity. *Am J Physiol Heart Circ Physiol*. 2001;281:H2597-2603.

35. Laurita KR, Rosenbaum DS. Interdependence of modulated dispersion and tissue structure in the mechanism of unidirectional block. *Circ Res*. 2000;87:922-928.

36. Qu Z, Garfinkel A, Weiss JN. Vulnerable window for conduction block in a one-dimensional cable of cardiac cells, 1: Single extrasystoles. *Biophys J*. 2006;91:793-804.

37. Shaw RM, Rudy Y. Ionic mechanisms of propagation in cardiac tissue. Roles of the sodium and l-type calcium currents during reduced excitability and decreased gap junction coupling. *Circ Res*. 1997;81:727-741.

38. Rohr S, Kucera JP. Involvement of the calcium inward current in cardiac impulse propagation: Induction of unidirectional conduction block by nifedipine and reversal by bay k 8644. *Biophys J*. 1997;72:754-766.

39. Hou L, Hu B, Jalife J. Genetically engineered excitable cardiac myofibroblasts coupled to cardiomyocytes rescue normal propagation and reduce arrhythmia complexity in heterocellular monolayers. *PLoS One*. 2013;8:e55400.

40. Bursac N, Kirkton RD, McSpadden LC, Liau B. Characterizing functional stem cell-cardiomyocyte interactions. *Regen Med*. 2010;5:87-105.

Figure Legends:

Figure 1. Fabrication of homocellular (host or donor) and heterocellular (host-donor) strands. **A**, Microcontact printing techniques were used to generate coverslips containing 150 μm-wide fibronectin lines spaced 300 μm-apart that converged into a common zone on one end (**top**). Homocellular or heterocellular strands were created by adhering a two-compartment PDMS frame parallel or perpendicular to the fibronectin lines to allow separate seeding of host NRVMs and donor engineered excitable HEK293 cells (the well-coupled "ExF" or poorly-coupled "ExS" lines).

Figure 2. Optical mapping in host-donor strands. **A**, mCherry fluorescence in donor excitable cells (eg, ExFs) allowed precise identification of host-donor interface with NRVMs. **B**, Optical recording sites (circles) overlaid on top of cells stained with ANNINE-6plus voltage-sensitive dye. Note small round ExFs in contact with larger elongated NRVMs. Optical mapping revealed

progressive APD prolongation across the host-donor interface (representative traces shown from recording sites). Scale bar for sequence of traces at bottom = 75 ms. **C-D,** Representative isochrone maps of action potential activation (1 ms (**C**) or 2 ms (**D**) spacing), repolarization (10 ms spacing), and duration (APD, 10 ms spacing), as well as corresponding spatial profiles of activation and repolarization shown for a representative ExF-NRVM (**C**) or ExS-NRVM (**D**) strand. Shown is the 30th propagated AP during 2 Hz pacing. Position of host-donor interface is assigned the coordinate x=0 mm.

Figure 3. Effects of $BaCl_2$ on the shape of APD and RT profiles in host-donor strands. **A-C,** Average APD profiles across the ExF-NRVM (green) and ExS-NRVM (blue) interface in the presence of 0 (**A**), 25 (**B**), or 50 (**C**) μmol/L $BaCl_2$ with overlaid Boltzmann fit. **D-I,** Average height, width, and maximum slope (gradient, ∇) of APD (**D-F**) or RT (**G-I**) profile within host-donor strands during AP propagation at 2 Hz stimulation from the ExF or ExS end of the strand. *$P<0.05$, ***$P<0.001$; n=16-42 per group. All groups are statistically different ($P<0.05$) when comparing across $BaCl_2$ conditions.

Figure 4. Location of S2 conduction block in host-donor strands. **A-B,** Representative space-time plots during pacing from the ExF (**A**) or ExS (**B**) end of host-donor strand showing AP propagation (in 0 μmol/L $BaCl_2$) during longest S1-S2 interval (S1-S2$_{max}$) that resulted in block (150 ms in **A** and 200 ms in **B**). Dashed red line at x=0 mm indicates position of host-donor interface. **C-D,** Distance from site of S1-S2$_{max}$ block to host-donor interface (**C**) or site of maximum repolarization gradient (**D**); ***$P<0.001$, n=10 per group. **E,** Representative space-time plots in an ExS-NRVM strand showing shift in the S2 block position with decrease in S1-S2

interval. Dashed red line, host-donor interface; solid red line, site of S2 block. **F,** Distance of S2 block site from site of S1-S2$_{max}$ block as a function of S1-S2 interval. Lines show linear fits for individual strands (n=4 for ExF-NRVM, n=5 for ExS-NRVM); average slopes between ExF-NVRM vs. ExS-NRVM strands differ significantly ($P<0.001$).

Figure 5. Vulnerable window of conduction block in host-donor strands as a function of RT profile shape. **A-C,** Relationship between vulnerable time window for S2 block and shape parameters of RT profile, namely: height (**A**), width (**B**), and maximum gradient (**C**); linear regression fit lines are shown only for statistically significant correlations (see Table II in online-only Data Supplement). **D,** Average vulnerable time windows for S2 block in host-donor strands without or with BaCl$_2$ application. ***$P<0.001$, n=16-21 per group.

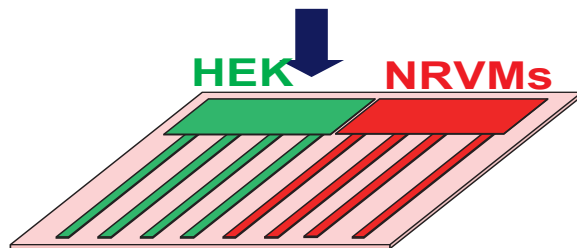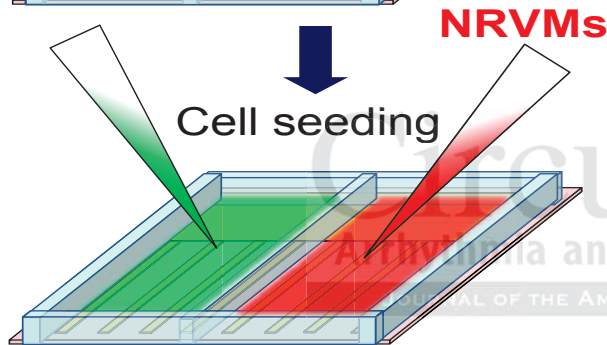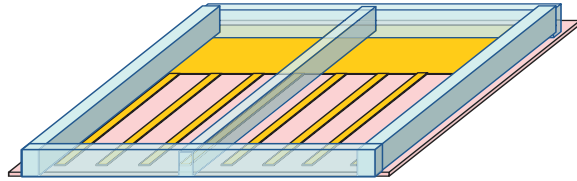**Figure 6.** S1-S2$_{max}$ in host-donor strands as a function of pacing location and BaCl$_2$ application. **A,** Representative space-time plots in an ExS-NRVM strand showing interface block when strand is paced at S1-S2=200 ms from the ExS end (left) but not NRVM end (right). **B,** Adding 50 µmol/L BaCl$_2$ yields successful conduction across the ExS-NRVM interface at S1-S2=200 ms with block now occurring at lower S1-S2=175 ms. **C,** S1-S2$_{max}$ for the local (left) or interface (middle) block when pacing from ExF (green) or ExS (blue) end, or local block when pacing from NRVM end (right) of the strand, without (lighter) and with (darker) addition of 50 µmol/L BaCl$_2$. Each line connects the three S1-S2$_{max}$ values measured in the same strand. Note that addition of BaCl$_2$ significantly increases S1-S2$_{max}$ for local block at the ExF and ExS end but not at the NRVM end of the strands, and significantly decreases S1-S2$_{max}$ for interface block in ExS-NRVM strands, but not in ExF-NRVM strands; n=5-10 per group, ***$P<0.001$ for ExF-NRVM

vs. ExS-NRVM interface block (denoted by black dashed line) and interface vs. local NRVM

pacing block in ExS-NRVM strands (denoted by light blue dashed line). Note that some data

points for the ExF-NRVM + 50 μM $BaCl_2$ and ExS-NRVM + 50 μM $BaCl_2$ groups overlap.
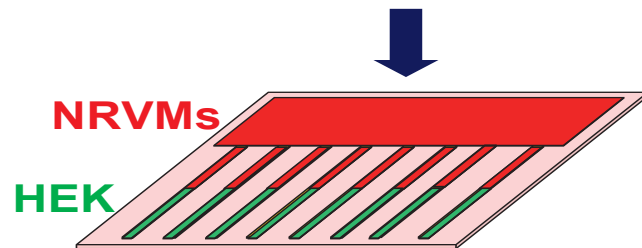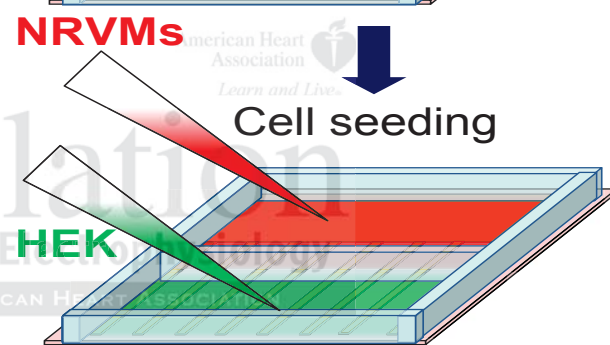
Homocellular Strands:
Adhere parallel PDMS frame

Heterocellular strands:
Adhere perpendicular PDMS frame

NRVMs

NRVMs

Cell seeding

Cell seeding

HEK

HEK | NRVMs

NRVMs

HEK

Homocellular Strands:

| NRVMs |
| ExF |
| ExS |

APD and CV Restitution Analysis
+/- 25 μM or 50 μM BaCl$_2$
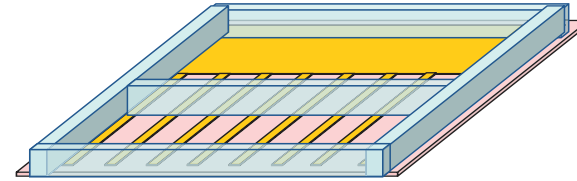
Heterocellular Strands:

| ExF | NRVMs |
| ExS | NRVMs |

Dispersion and Block Analysis
+/- 25 μM or 50 μM BaCl$_2$

A

S1-S2 = 200 ms   S1-S2 = 200 ms

Distance (mm): -.64, -.32, 0, .32, .64
Time (ms): 250, 500

ExS / NRVMs

B

S1-S2 = 200 ms   S1-S2 = 175 ms

Distance (mm): -.64, -.32, 0, .32, .64
Time (ms): 250, 500

ExS / NRVMs

C

S1S2 Interval (ms): 40, 60, 80, 100, 120, 140, 160, 180, 200, 220

- ExF-NRVM + 0 μM $BaCl_2$
- ExF-NRVM + 50 μM $BaCl_2$
- ExS-NRVM + 0 μM $BaCl_2$
- ExS-NRVM + 50 μM $BaCl_2$

***   ***

HEK293 pacing site block   Interface block   NRVM pacing site block